Lithospheric structure of the Canadian Shield inferred from inversion of surface-wave dispersion with thermodynamic a priori constraints

N.M. Shapiro[1], M.H. Ritzwoller[1], J.C. Mareschal[2], and C. Jaupart[3]

[1] Center for Imaging the Earth's Interior

Department of Physics, University of Colorado

Boulder, CO 80309-0390, USA

(e-mail: nshapiro@ciei.colorado.edu)

[2] GEOTOP-UQAM-McGill

Centre de Recherche en Géochimie et en Géodynamique

Université du Québec à Montréal

Montréal, Canada

[3] Institut de Physique du Globe de Paris

Paris, France

Manuscript submitted to: Geological Society of London Special Publication: *Geological Prior Information*, edited by Rachel Wood and Andrew Curtis, June 20, 2003.

Short title: LITHOSPHERIC STRUCTURE OF THE CANADIAN SHIELD

Abstract. We argue for and present a reformulation of the seismic surface wave inverse problem in terms of a thermal model of the upper mantle and apply the method to estimate lithospheric structure across much of the Canadian Shield. The reformulation is based on a steady-state temperature model, which we show to be justified for the studied region. The inverse problem is cast in terms of three thermal parameters: temperature in the uppermost mantle directly beneath Moho, mantle temperature gradient, and the potential temperature of the sublithospheric convecting mantle. In addition to the steady-state constraint, prior physical information on these model parameters is based on surface heat flow and heat production measurements, the condition that melting temperatures were not reached in the crust in Proterozoic times, and other theoretical considerations. We present the results of a Monte Carlo inversion of surface wave data with this "thermal parameterization" subject to the physical constraints for upper mantle shear velocity and temperature, from which we also estimate lithospheric thickness and mantle heat flux. The Monte Carlo inversion gives an ensemble of models that fit the data, providing estimates of uncertainties in model parameters. We also estimate the effect of uncertainties in the interconversion between temperature and seismic velocity. Variations in lithospheric temperature and shear velocity are not well correlated with geological province or surface tectonic history. Mantle heat flow and lithospheric thickness are anticorrelated and vary across the studied region, from 11 $mW/m^2$and nearly 400km in the northwest to about 24 $mW/m^2$and less than 150 km in the southeast. The relation between lithospheric thickness and mantle heat flow is consistent with a power law relation similar to that proposed by Jaupart et al. (1998) who argued that the lithosphere and asthenosphere beneath the Canadian Shield are in thermal equilibrium and heat flux into the deep lithosphere is governed by small scale sublithospheric convection.

1. Introduction

Studies of the structure, composition, and evolution of Precambrian continental lithosphere are the foundation of the current understanding of the processes that have shaped the growth and long-term stability of the continents. The thermal structure of Precambrian continental lithosphere has been studied principally with three methods: inversion of surface heat-flow measurements (e.g., Pollack et al., 1993; Nyblade and Pollack, 1993; Jaupart et al., 1998; Nyblade, 1999; Jaupart and Mareschal, 1999; Artemieva and Mooney, 2001), geothermobarometry of mantle xenoliths (e.g., a recent review by Smith, 1999), and seismic tomography (e.g., Furlong et al., 1995; Goes et al., 2000; Röhm et al., 2000). Each of these methods has distinct strengths and limitations. Thermobarometry of mantle xenoliths is probably most directly related to deep thermal structure, but high quality xenoliths are rare and those that are available have recorded the temperature of their formation which may not be representative of the current thermal regime of the lithosphere. In contrast, heat-flow measurements directly reflect the recent lithospheric thermal regime, but their ability to resolve the deep structure of the continental lithosphere is limited. Inverting surface heat-flow for the mantle geotherm requires strong a-priori assumptions about the thermal state of the lithosphere and on the distribution of heat sources. Seismic data are directly sensitive to the current deep structure of the lithosphere, but vertical resolution is limited and substantial uncertainties remain in the conversion from seismic velocity to temperature resulting particularly from ignorance of mantle composition and anelasticity.

The limitations of each of these methods individually lead naturally to exploiting them in combination. For example, Rudnick and Nyblade (1999) describe constraints on the Archean lithosphere that derive from applying xenolith thermobarometry and surface heat flow measurements simultaneously. Shapiro and Ritzwoller (2003) discuss the use of surface heat flux as an a priori contraint on inversions of seismic surface wave dispersion data. The heat flow measurements are used to establish upper and lower temperature bounds in the uppermost mantle directly beneath the Moho discontinuity. The temperature bounds are then converted to bounds on seismic velocity using the method of Goes et al. (2000). This approach can improve seismic models beneath continents, particularly beneath cratons and continental platforms, and tighten constraints on mantle temperatures. Shapiro and Ritzwoller

also describe an additional thermodynamic constraint that involves replacing ad-hoc seismic basis functions with a physical model of the thermal state of the upper mantle which is intrinsically a function of temperature. They applied this procedure to the oceanic upper mantle where the thermodynamic model consisted of a shallow conductive layer underlain by a convective mantle. They argued that the constraint produces more plausible models of the oceanic lithosphere and asthenosphere and reduces the uncertainty of the seismic model while negligibly degrading the fit to the seismic data.

This study is an extension of the results of Shapiro and Ritzwoller (2003) in two principal respects. First, Shapiro and Ritzwoller applied heat flow measurements as a prior constraint on seismic inversions only at a few isolated points to test the concept. In the present study, we apply the joint inversion over a wide region of North America, principally in the Canadian, where high quality heat flow measurements are available and the lithosphere is likely to be in thermal equilibrium. The locations of heat flow measurements used in this study are shown in Figure 1. We refer to these results as deriving from the "seismic parameterization", because models are constructed in seismic velocity model space. The heat flow constraints are converted to seismic velocities from temperature model space.

Heat flow measurements, however, do not cover the entire Canadian Shield, but are clustered mostly in southern Canada. To apply the heat flow constraint broadly across the Canadian Shield, therefore, would require us either to extrapolate existing measurements to other regions or to apply physical constraints derived from the regions where heat flow measurements exist. Here, we use the latter approach as the second extension of the results of Shapiro and Ritzwoller. Based on inversions in regions where heat flux measurements exist, we argue that the uppermost mantle beneath much of the studied region is likely to be in thermal steady-state; that is, the lithosphere is neither heating nor cooling and the surface heat flow is the sum of the heat entering the base of the lithosphere and the heat production in the crust. We reformulate the inverse problem in terms of a physical model of the thermal state of the upper mantle, in which a lithosphere in thermal steady-state overlies a convecting mantle. Models are constructed first in temperature model space and are tested to ensure that they satisfy the steady-state constraint, surface heat flow data (within uncertainties), and bounds on the mantle component of heat flow (discussed later). Temperature profiles that satisfy

these constraints are converted back to seismic model space where a seismic crust is introduced and the resulting model is tested to see if it fits the seismic data acceptably. We refer to these results as deriving from the "thermal parameterization". Figure 2 presents a schematic outline of the method based on the thermal parameterization. We apply this method to estimate the seismic and temperature structure of much of the Canadian Shield, including the mantle component of heat flux and lithospheric thickness.

Section 2 discusses the temperature bounds applied on the models based both on the seismic and thermal parameterizations. It also discusses uncertainties in the interconversion between temperature and seismic shear velocity. The joint inversion of surface wave dispersion and heat flow with the seismic parameterization is described in section 3. The inversion based on the thermal parameterization with the steady-state heat flow constraint is the subject of section 4. Finally, in section 5 we discuss the results of the inversion with the thermal parameterization, including estimates of lithospheric thickness and the mantle component of heat flow.

2. Bounds on Temperature and Seismic Velocities at the Top of the Mantle

2.1 Temperature bounds from heat flow

The assimilation of heat flow data in the seismic inverse problem is accomplished by constraining the uppermost mantle temperatures, T_m, estimated from surface heat flux. The Canadian Shield is an ideal location for the first extended application of this method for two reasons. First, the Canadian heat flow data (Figure 1) are of exceptional quality because, for example, heat flow has been measured using several deep neighboring boreholes in many cases (e.g., Jessop et al. 1984; Drury, 1985; Drury and Taylor, 1987; Drury et al., 1987; Mareschal et al., 1989; Pinet et al., 1991; Guillou et al., 1994; Hart et al., 1994; Guillou-Frottier et al., 1995, 1996; Mareschal et al., 1999, 2000; Rolandone et al., 2002) and there is an extensive data set of crustal heat production measurements (see Jaupart and Mareschal, 2003 for a review). Second, as discussed in detail by Shapiro and Ritzwoller (2003), the joint inversion of seismic data and heat flow is most straightforward for cold lithosphere such as that found beneath Precambrian

regimes. This is because uncertainties in the anelastic correction are smallest, which is part of the interconversion between temperature and seismic shear velocity. In addition, the volatile content, which can also affect the conversion to temperature, is believed to be small beneath ancient cratons due to the efficiency of partial melting upon their formation (e.g., Pollack, 1986).

Even in the best of cases, however, estimating temperatures at the top of the mantle requires determining the crustal geotherm, which depends on thermal conductivity and on the distribution of crustal heat production. Several methods have been used to determine radioactive heat production in the Canadian crust (e.g., Jaupart et al., 1998; Jaupart and Mareschal, 1999) and show that a simple linear relation between surface heat flow and crustal heat production is invalid because in many terranes, such as the greenstone belts, heat production is lower in the upper than in the mid crust. Lower crustal heat production is believed to be relatively homogeneous ($\sim$0.4 μW/m^3). Based on a simultaneous Monte Carlo inversion of heat flow and gravity data across the Abitibi belt, Guillou et al. (1994) proposed that the mantle component of heat flow lies between 7 and 15 mW/m^2. It has been suggested (e.g., Jaupart et al., 1998; Jaupart and Mareschal, 1999) that such low values for the heat flow from the mantle are characteristic of most of the Canadian Shield. The range was further narrowed down by Rolandone et al. (2002) who argued that mantle heat flow cannot be lower than 11 mW/m^{2}for the crust to have stabilized. We will use the assumption that heat flow from the mantle is relatively low and homogeneous across the region of study to compute crustal geotherms by solving the steady-state heat equation with different models of the distribution of heat production in the crust. The major cause for the uncertainties on the estimated temperature in the the upper mantle is the limited knowledge of crustal heat production.

To bound temperatures in the uppermost mantle we consider two end-member models of crustal heat production. The lower bound is set by a two layer crust that is consistent with a "cold" uppermost mantle with temperature T_{cold}. Heat production of 0.4μW/m^3 is used in the 20 km thick lower crust and upper crustal heat production is adjusted to match the measured surface heat flow with a constant mantle heat flow of 15 mW/m^2. We fix crustal thickness for the Canadian Shield at 40 km here (e.g., Perry et al., 2002) and crustal thermal

conductivity to 3.0 W $m^{-1}K^{-1}$. A second, single layer crustal model that produces a "hot" uppermost mantle with temperature T_{hot} was constructed by assuming that heat production is uniform throughout the crust with a value adjusted to the same constant mantle heat flow of 15 mW/m^2. The crustal thermal conductivity of 2.5 $Wm^{-1}K^{-1}$ is used for the "hot" model. The resulting two crustal geotherms for a surface heat flux of 45 mW/m^2 are shown in Figure 3.

In regions where the density of heat flow measurements is high, we use these bounds on uppermost mantle temperatures: $T_{min} = T_{cold}$ and $T_{max} = T_{hot}$. In regions away from heat flow measurements, however, we widen the temperature range by increasing the upper bound on temperature to $T_{max} = T_{hot} + (T_{hot} - T_{cold})$, but retain $T_{min} = T_{cold}$ because this lower bound is already very low. These bounds are varied spatially in a smooth way. Figure 4 displays the spatial variation of these temperature bounds in the uppermost mantle. The temperature limits T_{min} and T_{max} are sufficiently different to account for uncertainties in the crustal thermal parameters but still provide useful constraints on the seismic inversion, as demonstrated by the results below. As a final step, we interpolate the temperature bounds, T_{min} and T_{max}, onto the same $2^\circ \times 2^\circ$ geographical grid on which the surface wave dispersion maps are defined.

2.2 Interconversion between temperature and seismic velocity

We convert temperature to shear velocity using the method of Goes et al. (2000). This conversion is based on laboratory-measured thermoelastic properties of mantle minerals which are represented as partial derivatives of the elastic moduli with respect to temperature, pressure, and composition. The compositional model is the model of the old cratonic mantle proposed by McDonough and Rudnick (1998). This composition includes 83% Olivine, 15% Orthopyroxene, and 2% Garnet with an Iron content $X_{Fe} = 0.086$. For the anelastic correction, we follow Sobolev et al. (1996) and Goes et al. (2000):

$$Q_\mu(P,T,\omega) = A\omega^a \exp\left[a(H^* + PV^*)/RT\right] \quad (1)$$

$$v_{anel}(P,T,\omega) = v(P,T)\left[1 - \frac{2Q_\mu^{-1}(P,T,\omega)}{\tan(\pi a/2)}\right] \quad (2)$$

and set the exponent $a = 0.15$, activation energy $H^* = 500$ kJ/mol, and activation volume $V^* = 2.0 \times 10^{-5}$ m^3/mol, but as described in the appendix to Shapiro and Ritzwoller (2003) we set the amplitude $A = 0.049$ in contrast with their value of 0.148.

2.3 Uncertainties in the interconversion

Uncertainties in the seismic velocity-temperature relationship result from a number of sources, including uncertainties in mantle composition, in the thermoelastic properties of individual minerals, and in the anelastic correction which extrapolates anharmonic mineral properties measured in the laboratory to seismic frequencies. The physical properties of mantle minerals are measured in laboratories with high precision and are, therefore, not major contributors to errors in the velocity-temperature conversion. The most important uncertainties relate to mantle mineralogical composition and the anelastic correction. The presence of substantial quantities of melt and/or water in the mantle would also affect seismic velocities. These effects are expected to be negligible beneath old continental lithosphere, which is believed to have been largely dessicated during multiple episodes of melting during cratonic formation and is too cold for substantial quantities of melt currently to reside in the uppermost mantle.

To bound the effect of uncertainties in mantle mineralogical composition, we consider a pair of mantle compositional models proposed by McDonough and Rudnick (1998), one for on-cratonic (see section 2.2 above) and the other for off-cratonic (68% Olivine, 18% Orthopyroxene, 11% Clinopyroxene, and 3% Garnet with an Iron content $X_{Fe} = 0.1$) mantle. An assessment of the uncertainty in shear velocity coverted from temperature is shown in Figures 5a-c. We start with a input cratonic temperature model that is composed of a conductive steady-state linear geotherm with a sub-Moho temperature $T_m = 700K$ and mantle heat flow $Q_M = 15$ mW/m^{2}overlaying a 1573K adiabat (Figure 5a). This temperature model is converted to a shear velocity model using the method of Goes et al. (2000) applied to the on-cratonic and off-cratonic compositions, as shown in Figure 5b. The difference in the resulting shear-velocity curves provides a conservative estimate of the uncertainty in the temperature-velocity conversion within a single tectonic province.

We also consider two different models of the anelastic correction. Model Q_1 is the

model used by Shapiro and Ritzwoller (2003) and is described in section 2.2 above. For a contrasting model, we define Model Q_2 which is based on values taken from Berckhemer et al. (1982) from experiments on forsterite ($a = 0.25$, $A = 2.0 \times 10^{-4}$, $H^* = 584$ kJ/mol, $V^* = 2.1 \times 10^{-5}$ m^3/mol). These Q models are shown in Figure 6a computed from the temperature model in Figure 5a. Model Q_2 has weaker attenuation and, therefore, will have a smaller anelastic correction, as shown in Figure 6b, where the strength of the anelastic correction, is $2Q^{-1}/\tan(\pi a/2)$, by equation (2), These models represent fairly extreme values for the anelastic correction, so the difference in shear velocities obtained from these models provides a conservative estimate of uncertainties in the temperature-velocity conversion caused by our ignorance of Q.

Figure 5c shows that near to the surface, where the temperatures are relatively low and Q is high, the uncertainty in the anelastic correction is small and compositional uncertainty dominates. Deeper in the mantle, temperature increases, Q reduces, the anelastic correction strengthens and uncertainties in the anelastic correction become appreciably more important. Overall, the estimated uncertainty grows from about $\pm 0.5\%$ of the seismic velocity in the uppermost mantle near the Moho to about $\pm 1\%$ in the asthenosphere. A similar assessment of the uncertainty in temperature coverted from shear velocity is shown in Figures 5d-f. Again, uncertainty in composition dominates at shallow depths and uncertainty in Q is more important deeper in the upper mantle. The resulting uncertainty in temperature converted from shear velocity is about ± 100K at all depths.

It is important to account for these uncertainties in the inversions both with the seismic parameterization and the thermal parameterization presented below, because both involve interconversion between temperature and shear velocity. With the seismic parameterization, we convert the temperature bounds to bounds in seismic velocities explicitly. To account for the uncertainty of this conversion, we increase the range of seismic velocities by $\pm 0.5\%$ of the seismic velocity. The width of the bounds on seismic velocity, therefore, approximately doubles. With the thermal parameterization, trial models are constructed in temperature space so we introduce these uncertainties in the conversion to shear velocity by increasing the bounds on the temperature model parameters. We describe how we introduce these uncertainties into the range of allowed thermal parameters in section 4.1 below.

3. Joint Inversion: Seismic Parameterization

3.1 Inversion procedure

The seismic data set is composed of fundamental mode surface wave phase (Trampert and Woodhouse, 1996; Ekström et al., 1997) and group velocity (e.g., Ritzwoller and Levshin, 1998; Levshin et al., 2001) measurements that are used to produce surface-wave dispersion maps on a $2^\circ \times 2^\circ$ geographical grid using "diffraction tomography" (Ritzwoller et al., 2002), a method that is based on a physical model of lateral surface-wave sensitivity kernels. As described by Shapiro and Ritzwoller (2002), at each node of the grid, the Monte Carlo seismic inversion produces an ensemble of acceptable shear velocity models that satisfy the local surface wave dispersion information, as illustrated in Figure 7 for Spatial Point 1 (whose location is indicated on Figure 1). The model is radially anisotropic in the mantle ($V_{sv} \neq V_{sh}$) down to a depth of about 200 km, on average. The model is constructed to a depth of 400 km. We summarize the ensemble of acceptable seismic models with the "Median Model", which is the center of the corridor defined by the ensemble, and assign an uncertainty at each depth equal to the half-width of the corridor. When converting to temperature, we need the effective isotropic velocity in the upper mantle which we define as $V_s = (V_{sv} + V_{sh})/2$.

Figure 8 illustrates how assimilating heat flow information into the surface wave inversion affects the inversion at Point 1, which is located south of Hudson Bay within the Superior Province (see Figure 1). The heat flow constraint is shown in Figures 8a and 8b as a small box through which all models that satisfy the heat flow constraint must pass. In temperature space, this box has a width equal to the temperature extremes shown in Figure 4. In seismic velocity space, these extremes have been augmented by 0.5% in accordance with the estimate of the uncertainty in the conversion between temperature and seismic velocity described in section 2.3. The small box in Figures 9a-d shows this increase.

The models that fit the heat flow constraint are shown in Figures 8c and 8d and those that do not satisfy the constraint are shown in Figures 8e and 8f. Both the seismic and thermal models that fit the heat flow constraint are less oscillatory than those that do not satisfy the constraint. In the absence of the heat flow constraint, shear velocities display a minimum directly beneath the Moho and the geotherm exhibits a physically implausible minimum at

about 100 km depth. The introduction of the heat-flow constraint eliminates most of the models with this non-physical behavior, systematically favoring models with very high seismic velocities in the uppermost mantle directly beneath the Moho. This is consistent with the results of Lithoprobe refraction studies which have shown very fast P_n ($\approx$8.2 km s^{-1}) velocity beneath most of the Canadian Shield (e.g., Perry et al., 2002; Viejo and Clowes, 2003). In converting from seismic velocity to temperature in constructing Figures 8b, 8d, and 8f we have not included the uncertainty in the conversion from shear velocity to temperature. This uncertainty would widen the ensemble of temperatures somewhat.

Similar behavior can been seen at Points 2 and 3, located in northern Manitoba within the Trans-Hudson Orogen and in the Ungava Peninsula within the Superior Province, respectively (Figure 1). The results for these two sites are presented in Figures 9 and 10. In the Ungava Peninsula (Point 3), which is remote from heat flow measurements, the heat flow bounds on the seismic model are weaker and the seismic and temperature profiles displayed in Figures 10a and 10b are substantially more oscillatory and, hence, more physically questionable than those shown in Figures 8 and 9.

3.2 Characteristics of the upper mantle geotherm

As shown in Figures 8d, the temperature profiles that satisfy the heat flow constraint near heat flow measurements are consistent with a nearly linear shallow mantle geotherm. At Point 1, the temperature gradient $dT/dz \approx 5.5$ K/km which translates to a mantle heat flux $Q_M = kdT/dz \approx 16.5$ mW/m^2, for thermal conductivity $k = 3$ W m^{-1} K^{-1}. The linearity of the mantle geotherm is consistent with a "steady state" thermal regime with no mantle heat sources. The shallow geotherm in Figure 8d displays a knee at about 200 km, below which the geotherm has a different nearly linear temperature gradient. This gradient, $\approx$ 0.5K/km is similar to the mantle adiabatic gradient. The shallower temperature gradient defines a thermal boundary layer whose thickness we will refer to as the lithospheric thickness. The definition of "lithospheric thickness" is somewhat arbitrary, but for simplicity we will define it as the depth where the shallow linear gradient intersects the mantle adiabat. For Point 1 (8d), therefore, lithospheric thickness is estimated to be about 200 km. The main sources of errors in this estimate are due to uncertainties in the shallow geothermal gradient and in the potential

temperature of the convecting mantle (i.e. the horizontal position of the mantle adiabat).

Figures 9 and 10 present two wrinkles in characterizing the mantle geotherm. In Figure 9, which shows the results for the Trans Hudson Orogen (Point 2), the lithosphere is so thick that the transition to the mantle adiabat is not observable. Thus, lithospheric thickness cannot be directly constrained, more than by a lower bound of about 300 km. Mantle heat flux, however, is fairly well constrained to be about 11 $mW/m^2$and the temperature gradient is consistent with thermal steady-state. At Point 3, in the Ungava Peninsula away from heat flow measurements(Figure 10), the vertical oscillations in the temperature profile make it difficult to estimate either the mantle heat flux, lithospheric thickness, or to test the steady-state hypothesis.

The problems exemplified by Figures 9 and 10 motivate us to apply further constraints in the inversion that are based on tightening physically reasonable bounds on allowed temperature models. These constraints are designed to allow us to obtain better estimates of mantle heat flux and lithospheric thickness.

4. Joint Inversion: Thermal Parameterization

4.1 Inversion procedure

Figures 9 and 10 motivate us to introduce a parameterization based on a physical model in thermodynamic steady-state. The linearity of the shallow mantle geotherm, which is consistent with the steady-state hypothesis, is a general feature of the seismic model near heat flow measurements. The physical model we have adopted is schematized in Figure 11. The thermal parameterization consists of a linear gradient in the shallow mantle over a deeper adiabatic gradient set equal to 0.5 K/km. These two gradients meet in a narrow transition region to eliminate a kink in the temperature profile. The Monte-Carlo procedure randomly generates three numbers: the mantle temperature directly beneath Moho (T_m), the shallow mantle temperature gradient (dT/dz), and the potential temperature (T_p). Uppermost mantle temperature and the shallow gradient define the lithospheric geotherm. The potential temperature (i.e., the upward continuation of the adiabatic temperature profile to the surface) sets temperatures in the asthenosphere. Lithospheric thickness, L, is defined by the intersection

between the lithospheric geotherm and the adiabat. Other parameters could also be varied within some bounds, for example the adiabatic gradient, but doing so does not significantly increase the range of temperature profiles retained. As with the seismic parameterization, the inversion is performed at each point on a $2^\circ \times 2^\circ$ grid across the region of study.

Each of the three parameters is subjected to a constraints. First, the uppermost mantle temperature is within the same temperature bounds as for the seismic inversion, $T_{max} \leq T_m \leq T_{min}$, where T_{max} and T_{min} are shown in Figure 4. This constraint remains tightest near the heat flow measurements. In accordance with Figure 5, to account for uncertainty in the conversion to shear velocity, we increase these bounds by $\pm 0.5\%$ in the seismic velocity, as was also done in Figure 9a-d. Second, following Rolandone et al. (2002), lithospheric heat flux $Q_M = kdT/dz$ is constrained to be larger than 11 mW/m^2. It is also constrained to be less than surface heat flux, Q_s. Thus, 3.67 K/km $\leq T/dz \leq Q_s/k$, where thermal conductivity $k = 3.0$ W m^{-1}K^{-1}. Finally, the range of allowed potential temperatures is somewhat difficult to quantify. McKenzie and Bickle (1988) have proposed a mean upper mantle potential temperature of 1280°C and Jaupart et al. (1998) argue that uncertainties in this value are at least $\pm 50^\circ$C. The mean value beneath continents may be somewhat lower than the value proposed by McKenzie and Bickle. To be conservative, we extend the range somewhat and apply the following intrinsic bounds on potential temperature: 1100°C $\leq T_p \leq$ 1300°C. To account for uncertainty in the temperature to shear velocity conversion, we expand these bounds by $\pm 100^\circ$C to 1000°C $\leq T_p \leq$ 1400°C.

One of the principal advantages of the thermal parameterization is the possibility to apply physically based constraints on the model parameters. Although the bounds on potential temperature are poorly known, the lower bound of 11 mW/m^{2}on mantle heat flow strongly constrains the seismic model.

After a trial model is constructed in temperature space, it is converted to shear velocity using the method of Goes et al. (2000). Trial seismic crustal structures are introduced as well as mantle radial anisotropy similar to the generation of these features of the model in the seismic parameterization. At each grid node, some temperature profiles will be rejected entirely, but some will be found to fit the seismic data acceptably for an appropriate subset of seismic crustal models and models of radial anisotropy. These profiles define an ensemble of

acceptable profiles in temperature space. They are also combined with the crustal and radial anisotropic models to define an ensemble of acceptable models in seismic space.

Results for Points 1 and 3 (Figure 1) are shown in Figure 12. At Point 1, the results are very similar to those obtained with the seismic parameterization (Figures 8b,d). The estimated average mantle component of heat flow is 15 mW/m^{2}and its standard deviation is 2.0 mW/m^2. Average lithospheric thickness is 246 km with a standard deviation of 33 km. At Point 3, the thermal parameterization yields an ensemble of models that fit the surface wave data but do not display the physically questionable vertical oscillations that appear in Figure 10. The estimated average mantle heat flow and average lithospheric thickness are 12.2 mW/m^{2}and 294 km with corresponding standard deviations of 1.4 mW/m^{2}and 46 km.

4.2 Seismic and thermal models

The middle of the ensemble of acceptable models in the seismic and temperature model spaces are the Median Models. Slices of the Median Models of shear velocity and temperature are shown in Figures 13 and 14. Although shear velocity and temperature are fairly homogeneous at 80 km depth, at larger depths the variability is greater reflecting variations in lithospheric thickness across the study area, as discussed further below. The lithosphere is warmer and thinner to the south-east, in the Appalachians, and it becomes thicker toward the north and, especially, toward the north-west. Vertical oscillations that plague the seismic parameterization are absent from the model, as the cross sections in Figure 14 attest.

4.3 Mantle heat flux and lithospheric thickness

At each point, we construct an ensemble of mantle heat flow (Q_M) and lithospheric thickness (L) estimates derived from the ensemble of acceptable temperature profiles ($Q_M = kdT/dz, L =$ depth where the lithospheric geotherm intersects the mantle adiabat). The average of the ensemble of acceptable mantle heat flow and lithospheric thickness estimates is shown in Figure 15.

We assign uncertainties to Q_M and L equal to the standard deviation of the ensemble of acceptable values. Figure 16a shows that the uncertainty in mantle heat flow is greatest when mantle heat flow is high. This is because for a 1mW/m^{2}change there is a bigger change

in the temperature profile when heat flow is low (nearly vertical temperature profile) than when it is high (steep temperature profile). It appears that the uncertainty saturates at 2.5 mW/m^2. Figure 16b shows that the uncertainty in lithospheric thickness is also greatest for the thickest lithosphere. This is because the lithospheric temperature gradient and the slope of the mantle adiabat are almost equal. The uncertainty increases almost linearly with lithospheric thickness, but becomes much more scattered for thick lithosphere.

5. Discussion

The seismic velocities and temperatures displayed in Figures 13 and 14 demonstrate considerable variability across the study area. This information is probably best summarized by mantle heat flow and by the lithospheric thickness, as shown in Figure 16. The mantle heat flow appears to increase and lithospheric thickness to decrease beneath the Appalachians to the south east. Within the Canadian Shield, mantle heat flow from seismic inversions ranges between 11 and 18mW/m^2, with apparently higher values in the Grenville Province. Within most of the Superior Province, mantle heat flow ranges between 11 and 15 mW/m^2, with small amplitude, short wavelength (<1000km) spatial variations. Because of horizontal diffusion of heat, such variations in mantle heat flow are damped at the surface and can not be resolved by the heat flow data. Pinet et al. (1991) had concluded from their analysis of heat flow and heat production data that the mantle heat flow is the same beneath the Grenville and the Superior Province. Within the Canadian Shield, the variations are not always well correlated with geological provinces. The lowest mantle heat flow values are found beneath the Archean Rae Province and the Paleo-Proterozoic Trans Hudson Orogen, in northern Manitoba and Saskatchewan, where juvenile crust is thrust over the Archean Sask craton. Although the thermal regime of the Canadian Shield does not simply reflect its surface geology and is not simply related to the last tectonomagmatic event, it reveals the deeper structure of the lithosphere.

Patterns of lithospheric variability do emerge, however. As Figure 17 shows, lithospheric thickness and mantle heat flow are anticorrelated. A scaling law between mantle temperature and heat flow from the convecting mantle was used by Jaupart et al. (1998) to determine the lithospheric thickness. The analysis assumes that the heat flux at the base of the lithosphere

is supplied by small-scale convection (e.g., Davaille and Jaupart, 1993), and results in an approximately power-law relation between mantle heat flow and lithospheric thickness. Results of our seismic inversion shown in Figure 17 are also well approximated by a power law curve (Figure 17) that is relatively close to the shape of the $Q_M - L$ relationship given by Jaupart et al. (1998). However, Jaupart et al. (1998) pointed out that changes in lithospheric thickness do not require changes in mantle heat flow and that Moho temperatures (determined also by crustal heat production) also control lithospheric thickness. This is consistent with Figure 17 showing much more variability in lithospheric thickness than in mantle heat flow.

Acknowledgments

The phase velocity measurements used in the inversion were generously donated by Jeannot Trampert at Utrecht University and Michael Antolik, Adam Dziewonski, and Goran Ekström at Harvard University. All maps were generated with the Generic Mapping Tools (GMT) data processing and display package (Wessel and Smith, 1991; Wessel and Smith, 1995). This work was supported in part by a grant from the US National Science Foundation, NSF-OPP-0136103. JCM is grateful for the continuous support of NSERC (Canada) through a discovery grant.

References

Artemieva, I.M. and Mooney, W.D., 2001. Thermal thickness and evolution of Precambrian lithosphere: A global study, *J. Geophys. Res.,* **106**, 16,387-16,414.

Berckhemer, H., W. Kampfman, E. Aulbach, and H. Schmeling, 1982. Shear modulus and Q of forsterite and dunite near partial melting from forced oscillation, experiments, *Phys. Earth Planet. Inter.*, **29**, 30-41.

Doin, M.P. & L. Fleitout, 1996. Thermal evolution of the oceanic lithosphere: An alternative view, *Earth Planet. Sci. Lett.*, **142**, 121-136.

Drury, M.J., 1985. Heat flow and heat generation in Churchill Province of the Canadian Shield and their paleotectonic significance, *Tectonophys.*, **115**, 25-44.

Drury, M.J. & A.E. Taylor, 1987. Some new measurements of heat flow in the Superior Province of the Canadian Shield, *Can. J. Earth Sci.*, **24**, 1486-1489.

Drury, M.J., A.M. Jessop, & T.J. Lewis, 1987. The thermal nature of the Canadian Appalachians, *Tectonophys.*, **113**, 1-14.

Ekström, G., Tromp, J., & Larson, E.W.F., 1997. Measurements and global models of surface waves propagation, *J. Geophys. Res.,* **102**, 8137-8157.

Furlong, K.P, W. Spakman, and R. Wortel, 1995. Thermal structure of the continental lithosphere: constraints from seismic tomography, *Tectonophys., 244*, 107-117.

Guillou, L., J.C. Mareschal, C. Jaupart, C. Gariépy, G. Bienfait, & R. Lapointe, 1994 Heat flow gravity and structure of the Abitibi belt, Superior Province, Canada: Implications for mantle heat flow, *Earth Planet. Sci. Lett.*, **122**, 103-123.

Guillou-Frottier, L., J.C. Mareschal, C. Jaupart, C. Gariépy, R. Lapointe, & G. Bienfait, 1995. Heat flow variations in the Grenville Province, Canada, *Earth Planet. Sci. Lett.*, **136**, 447-460.

Guillou-Frottier, L., J.C. Mareschal, C. Jaupart, C. Gariépy, G. Bienfait, L.Z. Cheng, & R. Lapointe , 1996. High heat flow in the Thompson Belt of the Trans-Hudson Orogen, Canadian Shield, *Geophys. Res. Lett.,* **23**, 3027-3030.

Goes, S., Govers, R., & Vacher, R., 2000. Shallow mantle temperatures under Europe from P and S wave tomography, *J. Geophys. Res.,* **105**, 11,153-11,169.

Hart, S.R., J.S. Steinhart, & T.J. Smith, 1994. Terrestrial heat flow in Lake Superior, *Can. J. Earth. Sci.*, 31, 698-708.

Jaupart, C., J.C. Mareschal, L. Guillou-Frottier, & A. Davaille, 1998. Heat flow and thickness of the lithosphere in the Canadian Shield, *J. Geophys. Res.,* **103**, 15,269-15,286.

Jaupart, C. & J.C. Mareschal, 1999. The thermal structure and thickness of continental roots, *Lithos*, **48**, 93-114.

Jaupart, C. & J.C. Mareschal, 2003. Crustal heat production. *Textbook of Geochemistry, vol. 3, Composition of the Continental Crust*, edited by R. Rudnick, Elsevier Publishing Company, Amsterdam. in press.

Jessop, A.M., T.J. Lewis, A.S. Judge, A.E. Taylor, & M.J. Drury, 1984. Terrestrial heat flow in Canada, *Tectonophys.*, **103**, 239-261.

Kennett, B.L.N., Engdahl, E.R., & Buland, R., 1995. Constraints on seismic velocities in the Earth from travel times, *Geophys. J. Int.*, **122**, 403-416.

Levshin, A.L., M.H. Ritzwoller, M.P. Barmin, A. Villasenor, and C.A. Padgett, New constraints on the Arctic crust and uppermost mantle: Surface wave group velocities, Pn, and Sn, *Phys. Earth Planet. Int.*, 1 **23**, 185 - 204, 2001.

Mareschal, J.C., C. Pinet, C. Gariépy, C. Jaupart, C. Bienfait, G. Dalla-Coletta, J. Jolivet, & R. Lapointe, 1989. New heat flow density and radiogenic heat production data in the Canadian Shield and the Québec Appalachians, *Can. J. Earth. Sci.*, **26**, 845-853.

Mareschal, J.C., C. Jaupart, L.Z. Cheng, F. Rolandone, C. Gariépy, C. Bienfait, L. Guillou-Frottier, & R. Lapointe, 1999. Heat flow in the Trans-Hudson Orogen of the Canadian Shield: Implications for Proterozoic continental growth, *J. Geophys. Res.,* **104**, 29,007-29,024.

Mareschal, J.C., A. Poirier, F. Rolandone, G. Bienfait, C. Gariépy, R. Lapointe, & C. Jaupart, 2000. Low mantle heat flow at the edge of the North American continent, Voisey Bay, Labrador, *Geophys. Res. Lett.,* **27**, 823-826.

McDonough, W.F. & Rudnick, R.L., 1998. *Mineralogy and composition of the upper mantle*, in: Ultrahigh-pressure mineralogy: physics and chemistry of the Earth's deep interior, R.J. Hemley, Editor, Mineralogical Society of America, Washington, DC.

McKenzie, D.P. and M.J. Bickle, 1988. Volume and composition of melt generated by extension of the lithosphere, *J. Petrol., 29*, 625-679.

Nyblade, A.A., 1999. Heat flow and the structure of the Precambrian lithosphere, *Lithos, 48*, 81-91.

Nyblade, A.A. & Pollack, H.N., 1993. A global analysis of heat flow from Precambrian terrains: implications for the thermal structure of Archean and Proterozoic lithosphere, *J. Geophys. Res.,* **98**, 12,207-12,218.

Perry, H.K.C., D.W.S. Eaton, & A.M. Forte, 2002. LITH5.0: a revised crustal model for Canada based on Lithoprobe results, *Geophys. J. Int.*, **150**, 285-294.

Pinet, C., C. Jaupart, J.C. Mareschal, C. Gariépy, G. Bienfait, & R. Lapointe, 1991. Heat flow and structure of the lithosphere in the eastern Canadian Shield, *J. Geophys. Res.,* **96**, 19,941-19,963.

Pollack, H.N., 1986. Cratonization and thermal evolution of the mantle, *Earth Planet. Sci. Letts.*, **80**, 175-182.

Pollack, H.N., Hurter, S.J., & Johnson, J.R., 1993. Heat flow from the Earth's interior: analysis of the global data set *Revs. Geophys.*, **31**, 267-280.

Ritzwoller, M.H. & Levshin, A.L., 1998. Eurasian surface wave tomography: group velocities, *J. Geophys. Res.,* **103**, 4839-4878.

Ritzwoller, M.H., Shapiro, N.M., Barmin, M.P., & Levshin, A.L., 2002. Global surface wave diffraction tomography, *J. Geophys. Res.,* 107(B12), 2335.

Röhm, A.H.E., Snieder, R., Goes, S., & Trampert, J., 2000. Thermal structure of continental upper mantle inferred from $S-$wave velocity and surface heat flow, *Earth Planet. Sci. Lett.,* **181**, 395-407.

Rolandone, F., C. Jaupart, J.C. Mareschal, C. Gariépy, G. Bienfait, C. Carbonne, & R. Lapointe, 2002. Surface heat flow, crustal temperatures and mantle heat flow in the

Proterozoic Trans-Hudson Orogen, Canadian Shield, *J. Geophys. Res.,* **107**, 2341, ETG 7, 2002.

Rudnick, R.L., McDonough, W.F., & O'Connell, R.J., 1998. Thermal structure, thickness and composition of continental lithosphere, *Chemical Geology*, **145**, 395-411.

Rudnick, R.L. & A.A. Nyblade, 1999. The thickness and heat production of Archean lithosphere: constraints from xenoliths thermobarometry and surface heat flow, in: Mantle Petrology: Field Observations and High Pressure Experimentation: A Tribute to Francis R. (Joe) Boyd, The Geochemical Society, Special Publication, **6**, 3-12.

Russell, J.K., Dipple, G.M., & Kopylova, M.G., 2001. Heat production and heat flow in the mantle lithosphere, Slave craton, Canada, *Phys. Earth Planet. Inter.,* **123**, 27-44.

Shapiro, N.M. & Ritzwoller, M.H., 2002. Monte-Carlo inversion for a global shear velocity model of the crust and upper mantle, *Geophys. J. Int.*, **151**, 88-105.

Shapiro, N.M. & M.H. Ritzwoller, 2003. Thermodynamic constraints on seismic inversions, *Geophys. J. Int.*, submitted.

Smith, D., 1996. Temperatures and pressures of mineral equilibration in peridotite xenoliths: review, discussion, and implications. In *Mantle Petrology: Field Observations and High-Pressure Experimentation: A Tribute to Francis R. (Joe) Boyd*, (eds. Y. Fei, C.M. Bertka, and B.O. Mysen), The Geochemical Society.

Sobolev, S.V., Zeyen, H., Stoll, G., Werling, F., Altherr, R., & Fuchs, K., 1996. Upper mantle temperatures from teleseismic tomography of French Massif Central including effects of composition, mineral reactions, anharmonicity, anelasticity and partial melt. *Earth Planet. Sci. Lett.,* **157**, 193-207.

Trampert, J. & Woodhouse, J.H., 1995. Global phase velocity maps of Love and Rayleigh waves between 40 and 150 s period, *Geophys. J. Int.*, **122**, 675-690.

Viejo, G.F. & R.M. Clowes, 2003. Lithospheric structure beneath the Archean Slave Province and Proterozoic Wopmay orogen, northwestern Canada, from LITHOPROBE refraction/wide-angle reflection survey, *Geophys. J. Int.*, **153**, 1-19.

Wessel, P., and W.H.F. Smith, 1991. Free software helps map and display data, *Eos Trans. AGU, 72*, 441.

Wessel, P., and W.H.F. Smith, 1995. New version of the Generic Mapping Tools released, *Eos Trans. AGU, 76*, 329.

Received ; revised ; accepted .

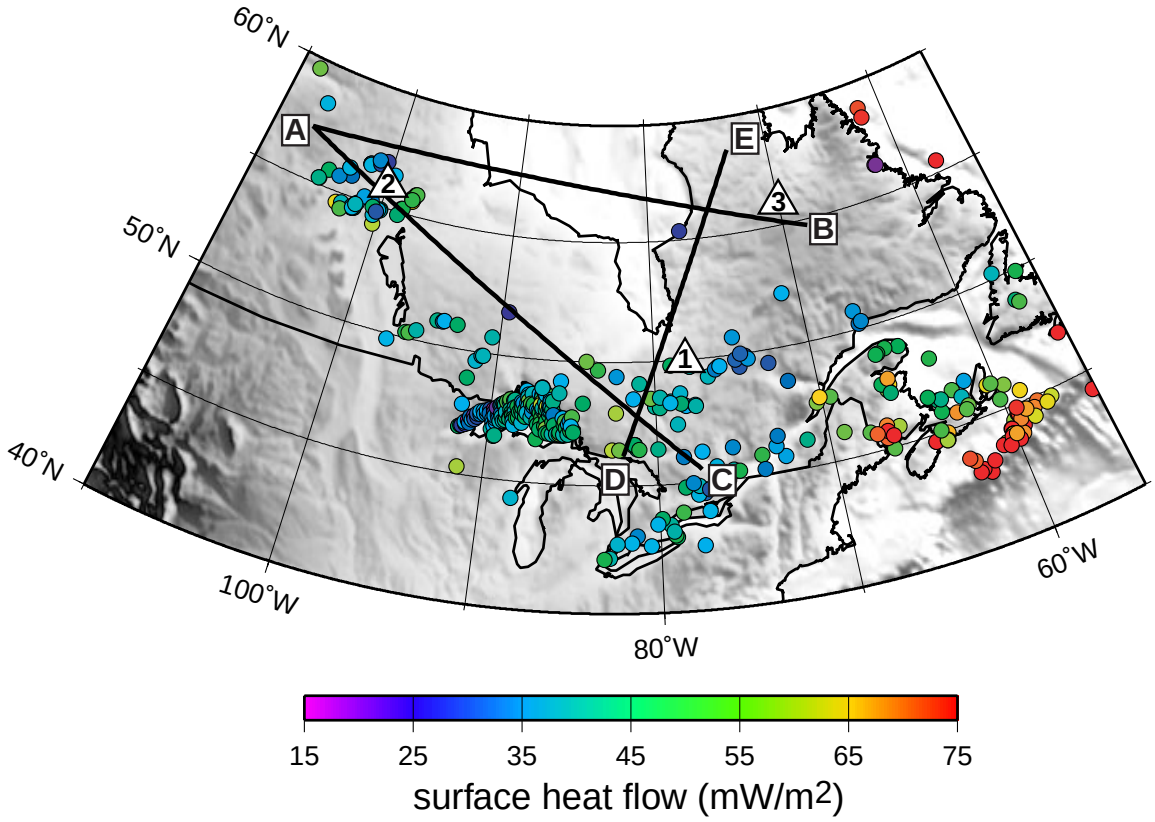

Figure 1. Reference map of eastern Canada showing the heat-flow measurements used in this study as well as the locations of the 1-D (Spatial Points 1, 2, 3) and 2-D profiles (A-B, A-C, D-E) referred to in the study.

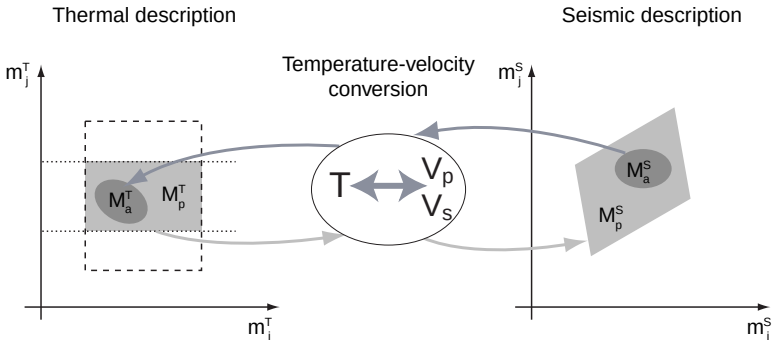

Figure 2. Schematic representation of the Monte-Carlo seismic inversion based on a thermal parameterization with a priori constraints. The thermal parameterization (left panel) is constrained by the heat-flow data (horizontal dotted lines) where they exist, the steady-state constraint on the thermal structure of the mantle (dashed rectangle), and a lower bound on mantle heat flow (not shown). These constraints delimit the range of physically plausible thermal models M_p^T (light shaded area on the left panel). Using a temperature-seismic velocity conversion, this range is converted into a range of physically plausible seismic models M_p^S (light shaded area on the right panel) to which a range of crustal seismic models and radial anisotropy are added. Random sampling within M_p^S identifies the ensemble of acceptable seismic models M_a^S (dark shaded area on the right panel). Finally, the seismic crust is stripped off and this ensemble is converted back into the ensemble of acceptable temperature models M_a^T (dark shaded area on the left panel).

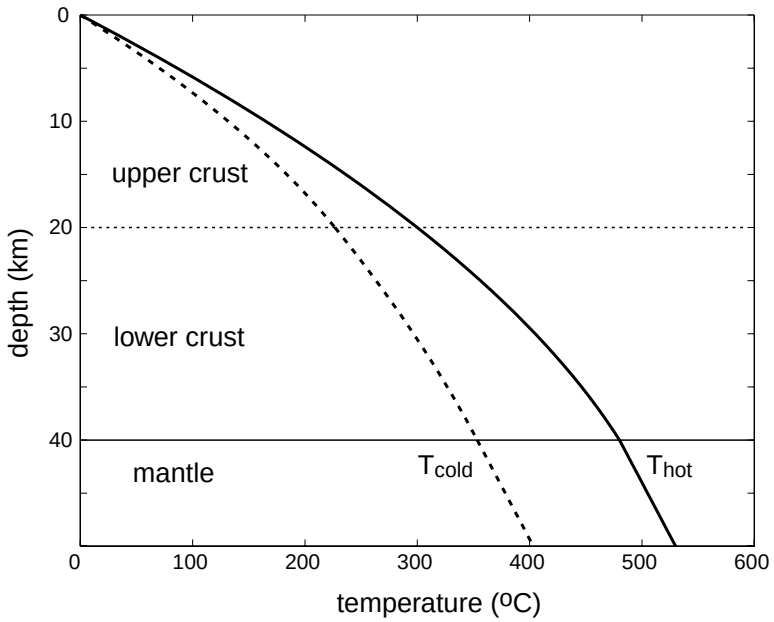

Figure 3. End-member crustal models that define T_{cold} and T_{hot} at the top of the mantle for a surface heat flux of 45 mW/m^2. For both models, the same values are assumed for the mantle heat flow and thermal conductivity.

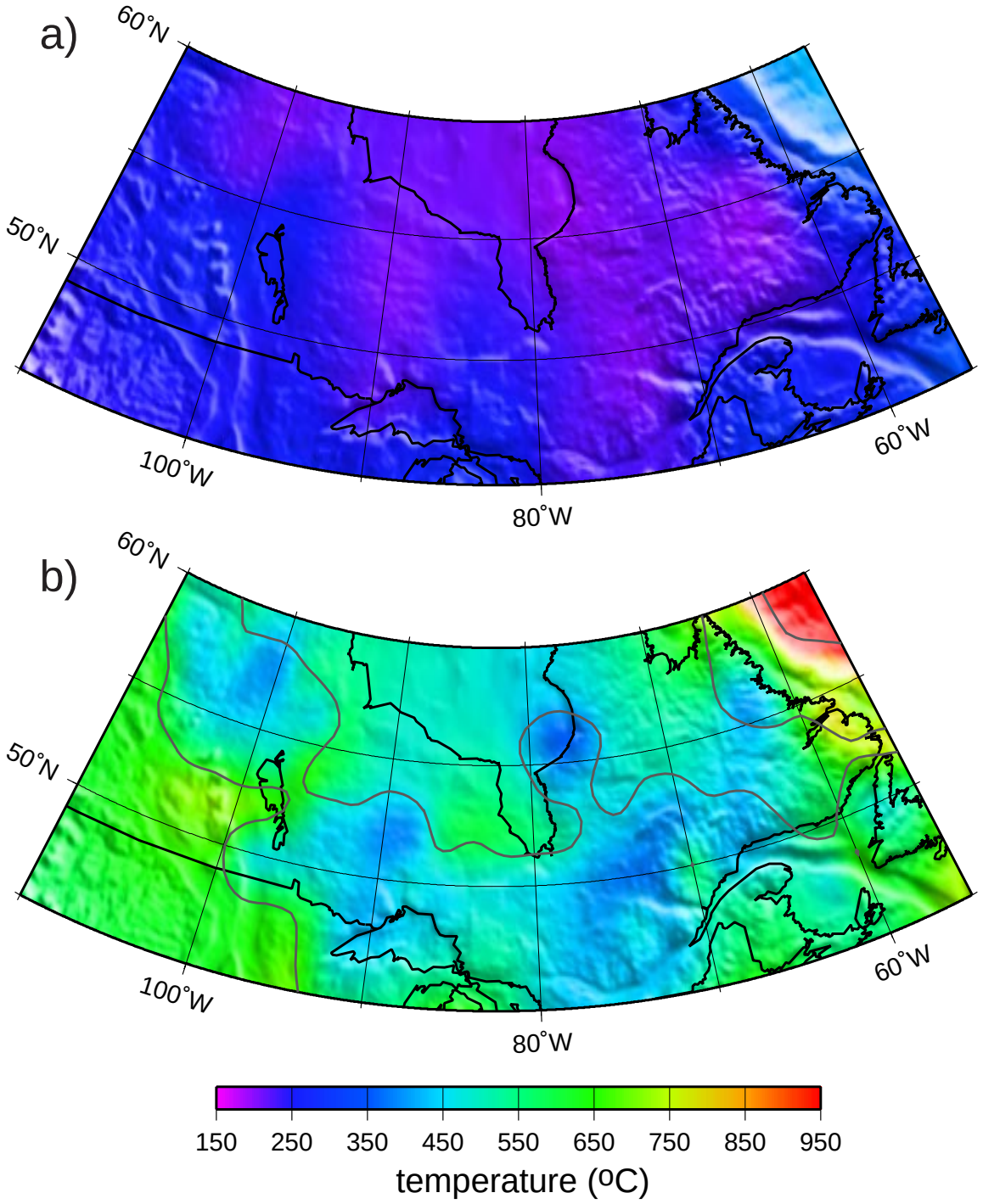

Figure 4. Uppermost mantle (sub-Moho) temperature bounds inferred from the heat flow data. (a) Lower bound T_{min}. (b) Upper bound T_{max}. The grey contour in (b) encircles the points within 200 km of a heat flow measurement. Temperature bounds are tightest near heat flow measurements.

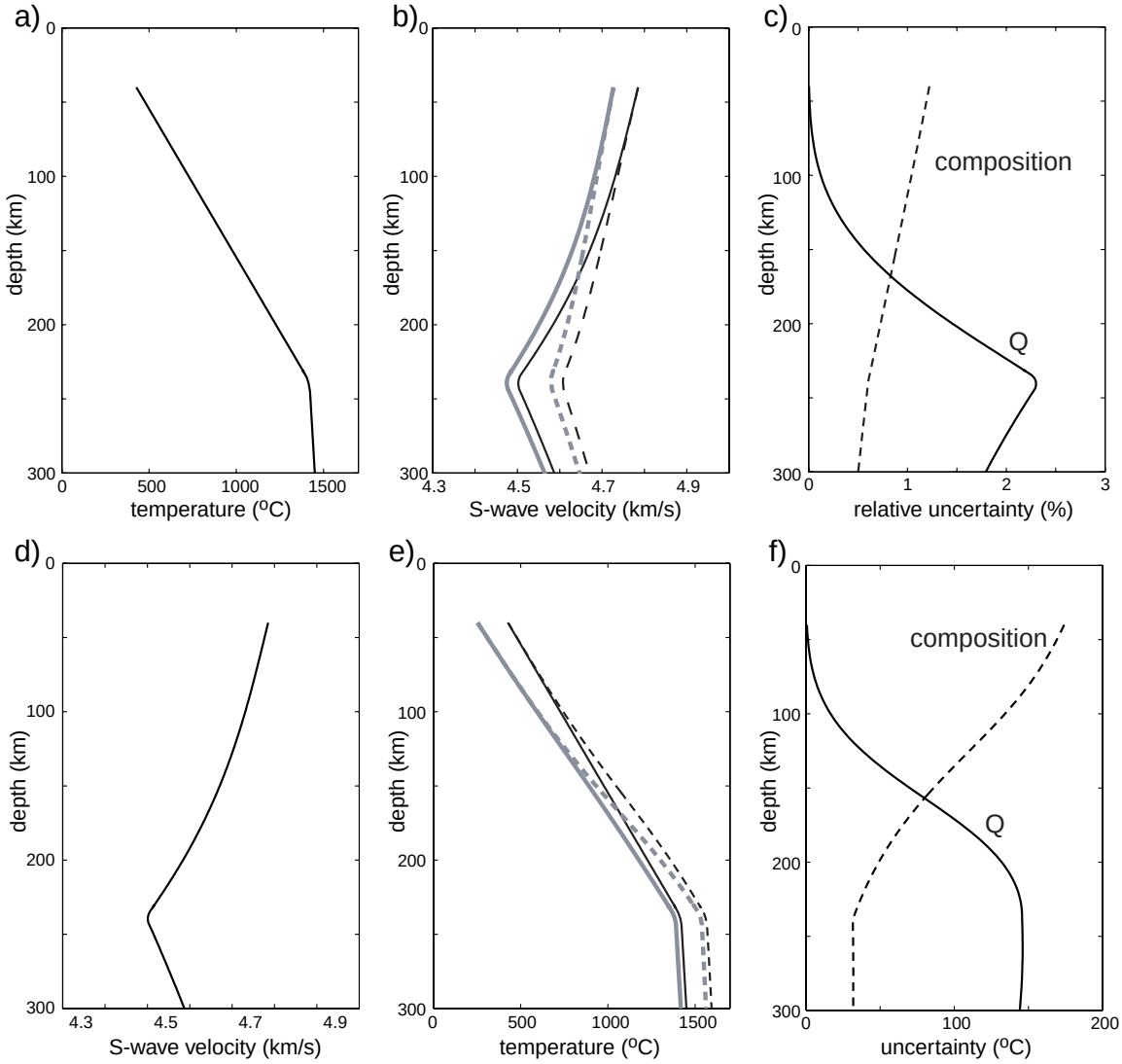

Figure 5. Assessment of uncertainties in the interconversion between temperature and shear velocity. (a) Input mantle temperature profile. (b) Shear velocity profiles converted from temperature with variable compositional and Q models. The black line and gray lines correspond to on-cratonic and off-cratonic compositions, respectively. The solid and dashed lines correspond to two mantle Q models, models Q_1 and Q_2 respectively. (c) Relative uncertainties in the shear velocity produced by uncertainties in composition (dashed line) and Q (solid line). (d) Input mantle shear velocity profile. (e) Temperature profiles converted from shear velocity with variable compositional and Q models, as in (b). (f) Relative uncertainties in temperature produced by uncertainties in composition (dashed line) and Q (solid line).

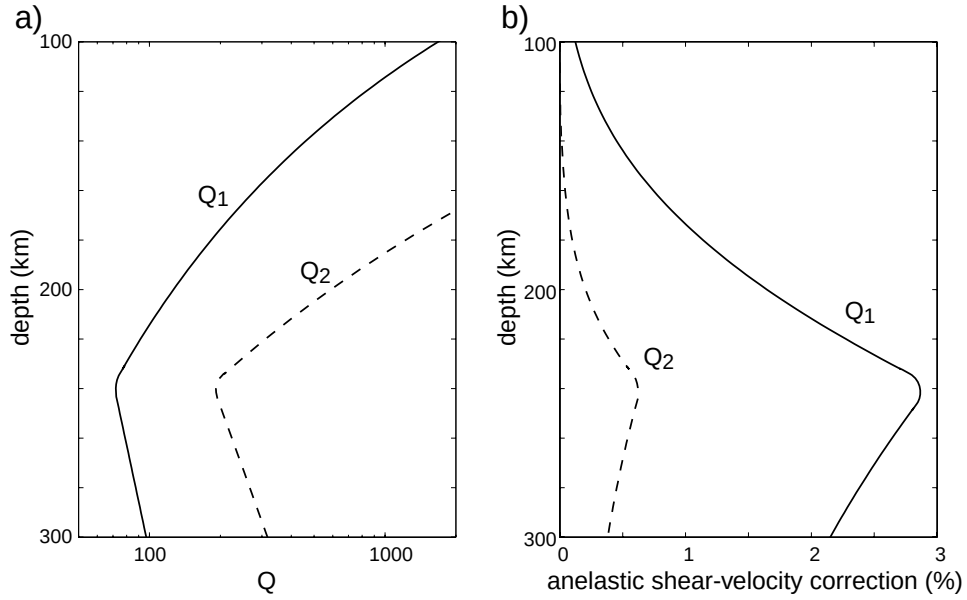

Figure 6. (a) Two alternative Q models, Q_1 and Q_2, described in the text, plotted here for the temperature profile shown in Figure 5a. (b) The strength of the anelastic correction from models Q_1 and Q_2, presented as the percent perturbation to the anharmonic shear velocity. In both figures, the solid line corresponds to Model Q_1 and the dashed line to Model Q_2.

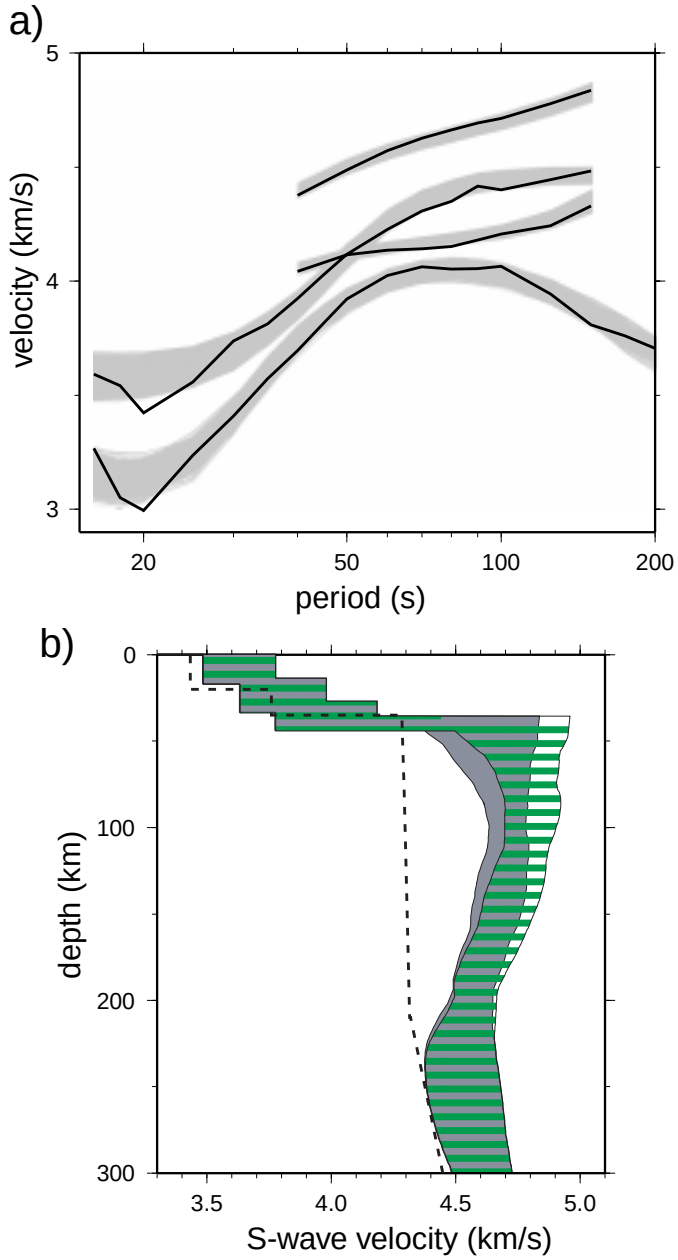

Figure 7. Monte Carlo inversion with the seismic parameterization, but without thermodynamic constraints . (a) Surface wave dispersion curves (black lines) at Spatial Point 1 (whose location is indicated on Figure 1) and the range of curves (grey lines) predicted from the the constitutive seismic models in (b). (b) The ensemble of radially anisotropic models that acceptably fit the dispersion curves found in (a). The solid grey corridor is V_{sv} and the cross-hatched corridor is V_{sh}. The dotted line is V_s from the 1-D model ak135 (Kennett et al., 1995).

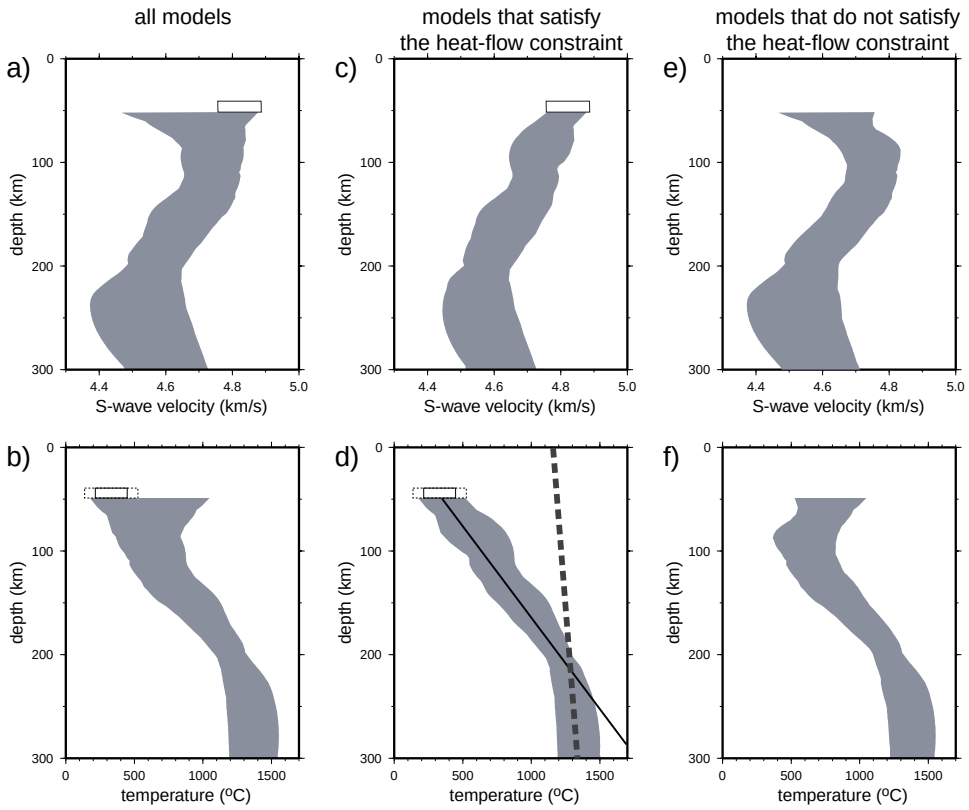

Figure 8. Results of the Monte-Carlo inversion with the seismic parameterization for the Superior Province south of Hudson Bay (Point 1 on Figure 1) illustrating the effect of the application of the heat flow constraint. (a) - (b) The ensemble of acceptable seismic ($V_s = (V_{sv} + V_{sh})/2$) and temperature models that fit the seismic dispersion curves acceptably. The small box at the top shows the bounds derived from heat flow. (c) - (d) The models that fit both the local dispersion curves and the heat flow constraint. (e) - (f) The models that fit the local dispersion curves but not the heat flow constraint. In (d), the best-fitting linear geotherm (solid line, $Q_M = 16.5$ mW/m^2) is shown as the solid line. The thick dashed line indicates the adiabat, whose horizontal offset is determined from the deep part of the temperature profile and whose vertical gradient is 0.5 °C/km.

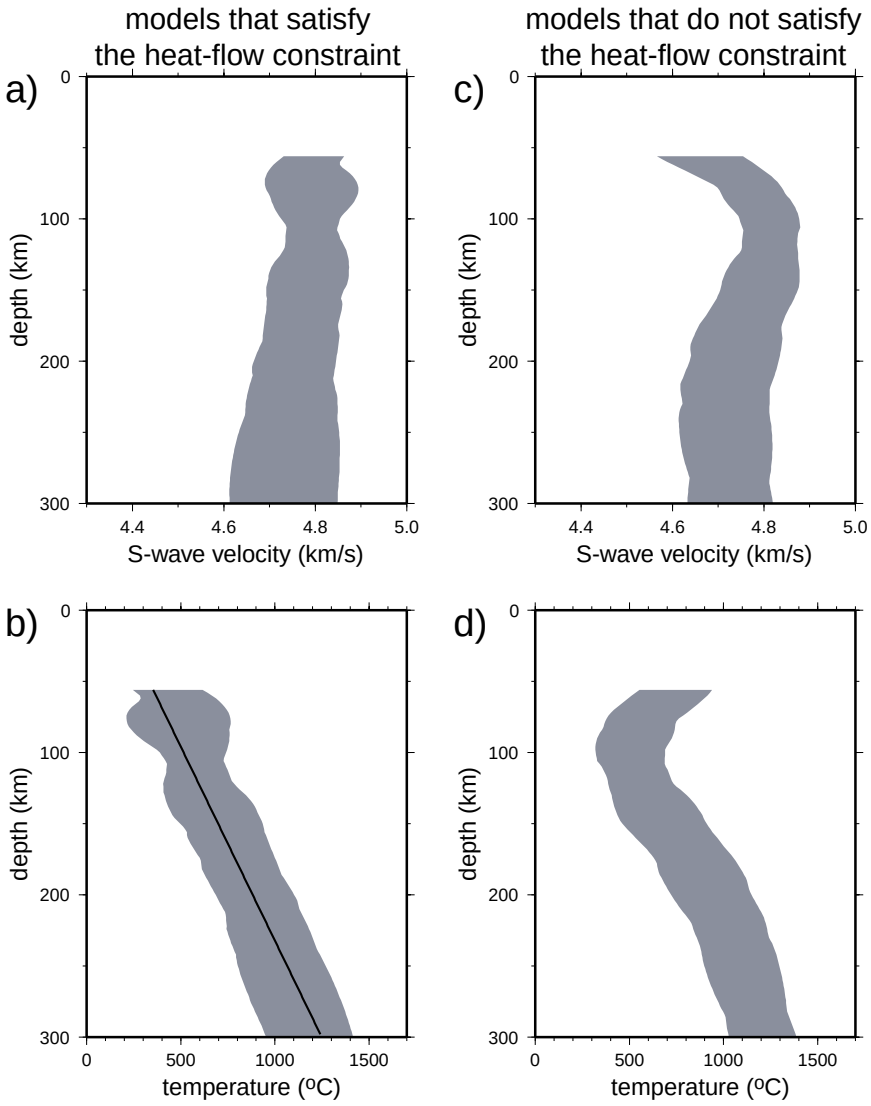

Figure 9. Results of the joint inversion with the seismic parameterization at the point in the Trans-Hudson Orogen (Point 2 in Figure 1). Here (a) - (b) are the models that fit both the local dispersion curves and the heat flow constraint and (c) - (d) are the models that do not fit the heat flow constraint. The mantle adiabat cannot be discerned, as the knee in the temperature profile appears to be deeper than the extent of the model (i.e., 300 km). As in Figure 8, in (b) the best-fitting linear geotherm ($Q_M = 11$ mW/m^2) is shown.

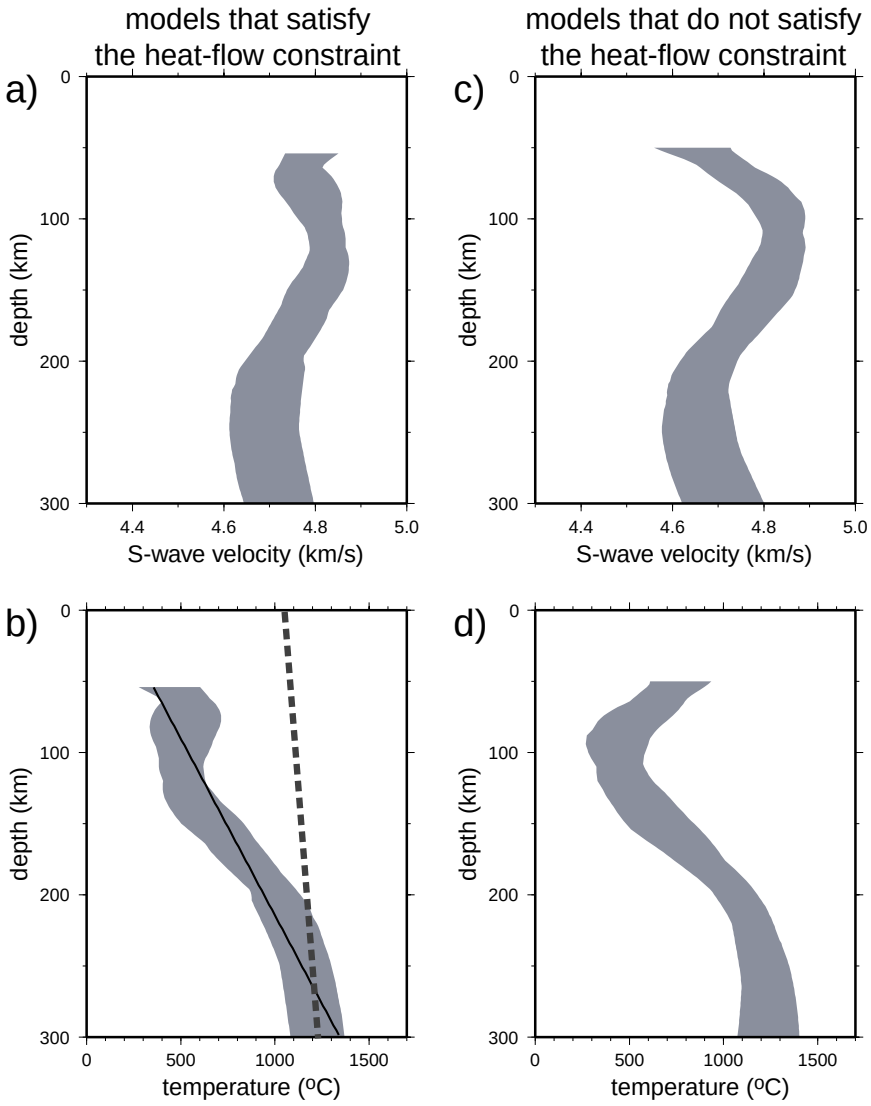

Figure 10. Results of the joint inversion with the seismic parameterization at the point in the Superior Province in the Ungava Peninsula of New Quebec (Point 3 in Figure 1). In contrast with Spatial Points 1 and 2, this point is remote from heat flow measurements which results in a weak heat flow constraint so that the the oscillations in the seismic and temperature profiles have not been eliminated. As in Figures 8 and 9, in (b) the best-fitting linear geotherm (solid line, $Q_M = 12$ mW/m^2) is shown with the mantle adiabat, but there are large uncertainties due to irregularities in the temperature profile with depth.

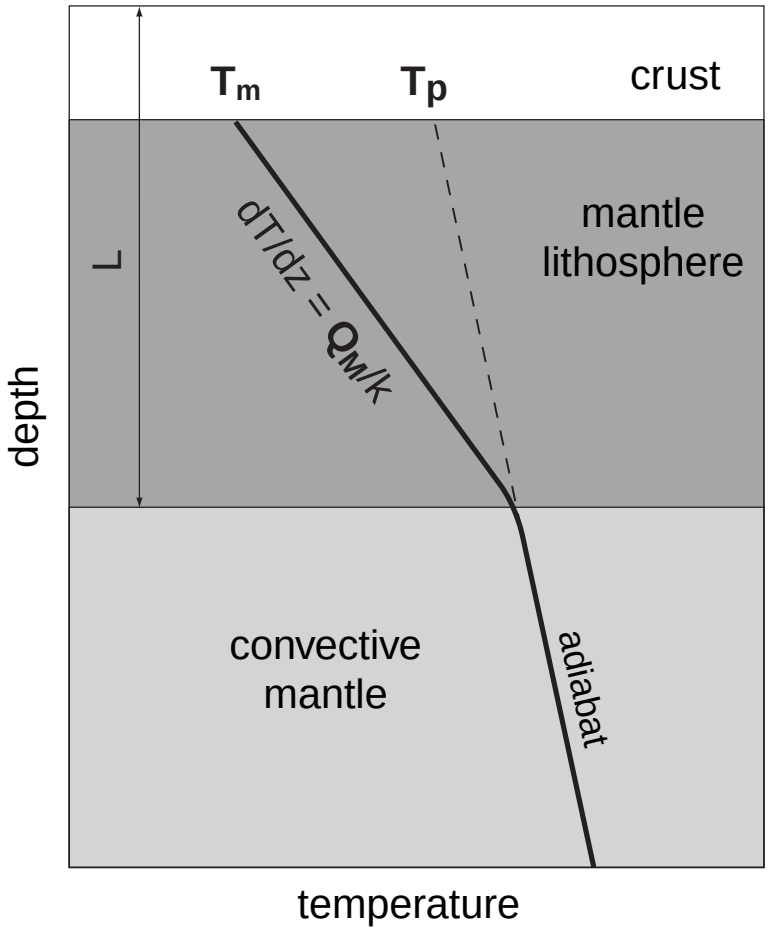

Figure 11. Schematic representation of the thermal model which is defines by three parameters. The steady-state lithospheric geotherm is defined by temperature directly beneath the Moho (T_m) and the linear gradient (dT/dz) which is simply related to mantle heat flow (Q_M). Below the lithosphere the temperature gradient is in the convecting mantle is adiabatic with potential temperature T_p and an adiabatic gradient of 0.5 K/km. These two gradients join smoothly through a narrow transition region in order to eliminate a non-physical kink in the temperature profile.

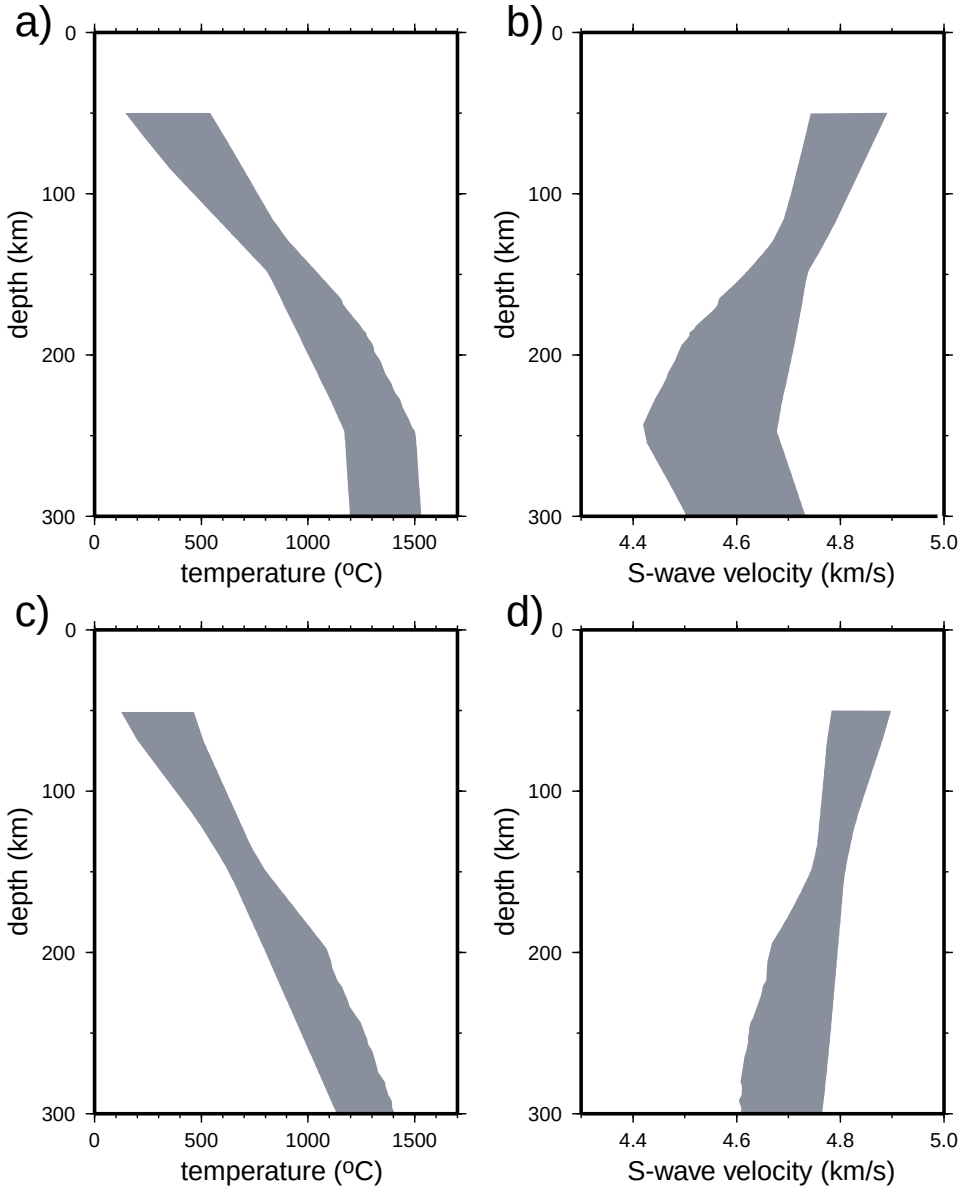

Figure 12. Example results of the Monte-Carlo inversion with the thermal parameterization at Spatial Points 1 and 3. (a) Ensemble of acceptable seismic models at Point 1. (b) Esemble of acceptable temperature models at Point 1. (c) Ensemble of acceptable seismic models at Point 3. (d) Ensemble of acceptable temperature models at Point 3.

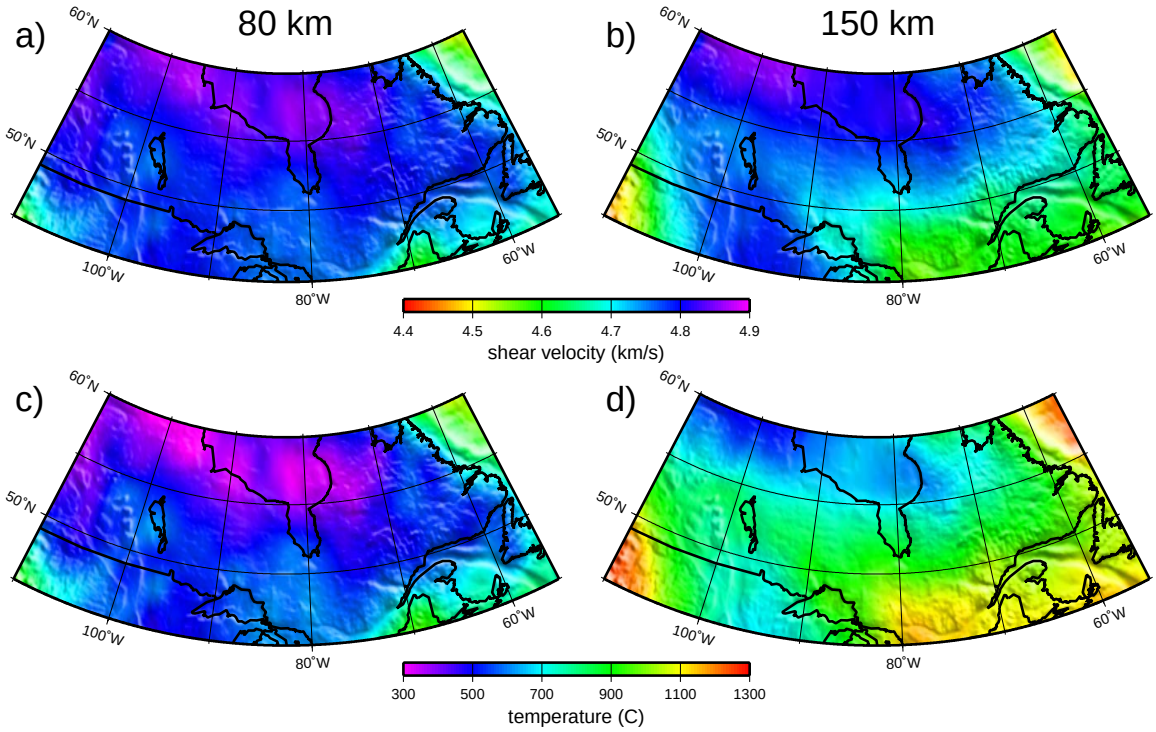

Figure 13. Horizontal slices of the seismic $V_s = (V_{sh} + V_{sv})/2$ model (a, b) and the temperature model (c, d) at depths of (a, c) 80 km and (b, d) 150 km.

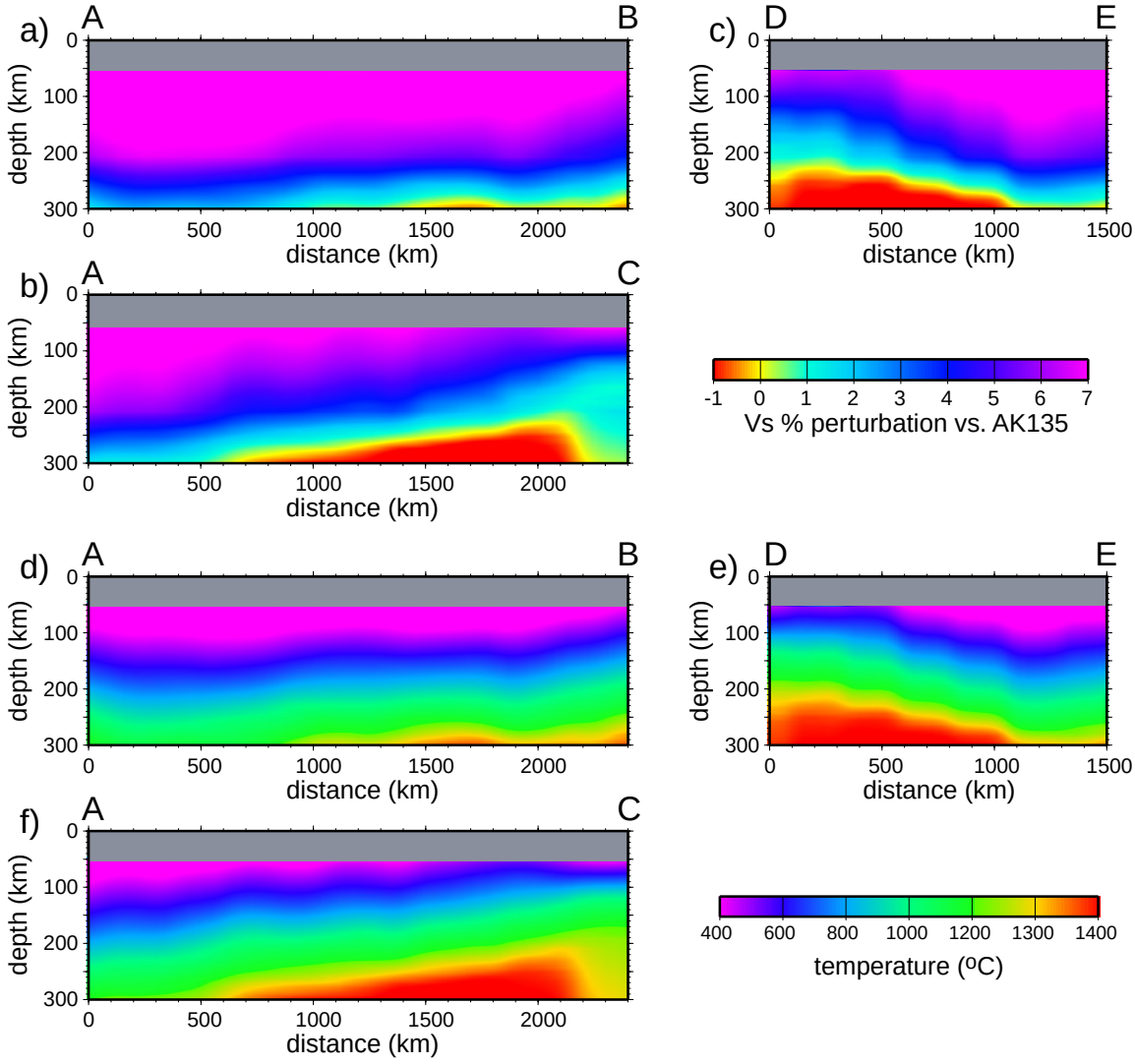

Figure 14. Vertical slices of the seismic and temperature models along the three profiles shown in Figure 1. (a) - (c) Isotropic shear velocity ($V_s = (V_{sh} + V_{sv})/2$) presented as percent perturbation relative to the global 1-D model ak135. (d) - (f) Temperature in $^{\circ}$C.

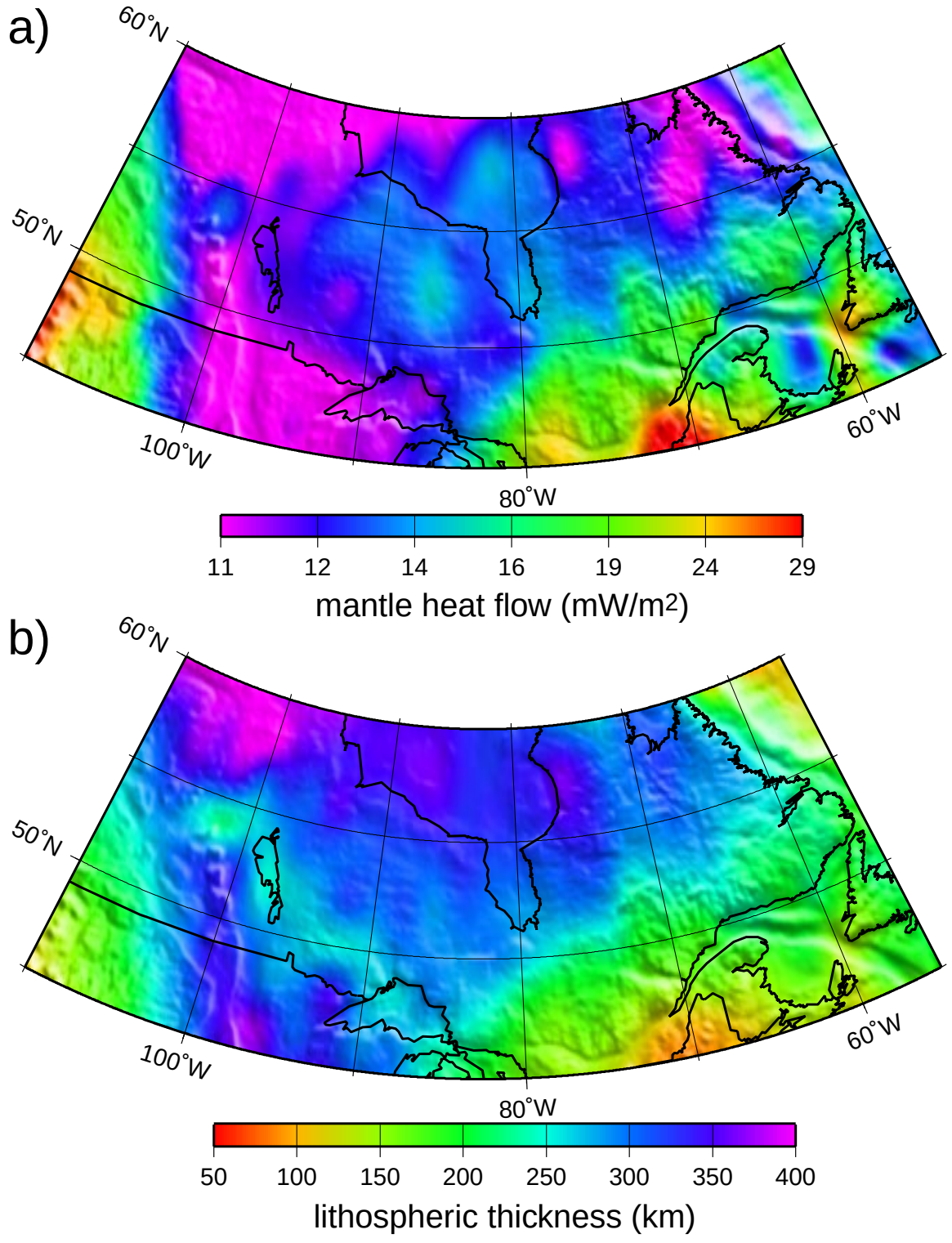

Figure 15. (a) The estimated mantle component of heat flow, Q_M. (b) The estimated lithospheric thickness, L.

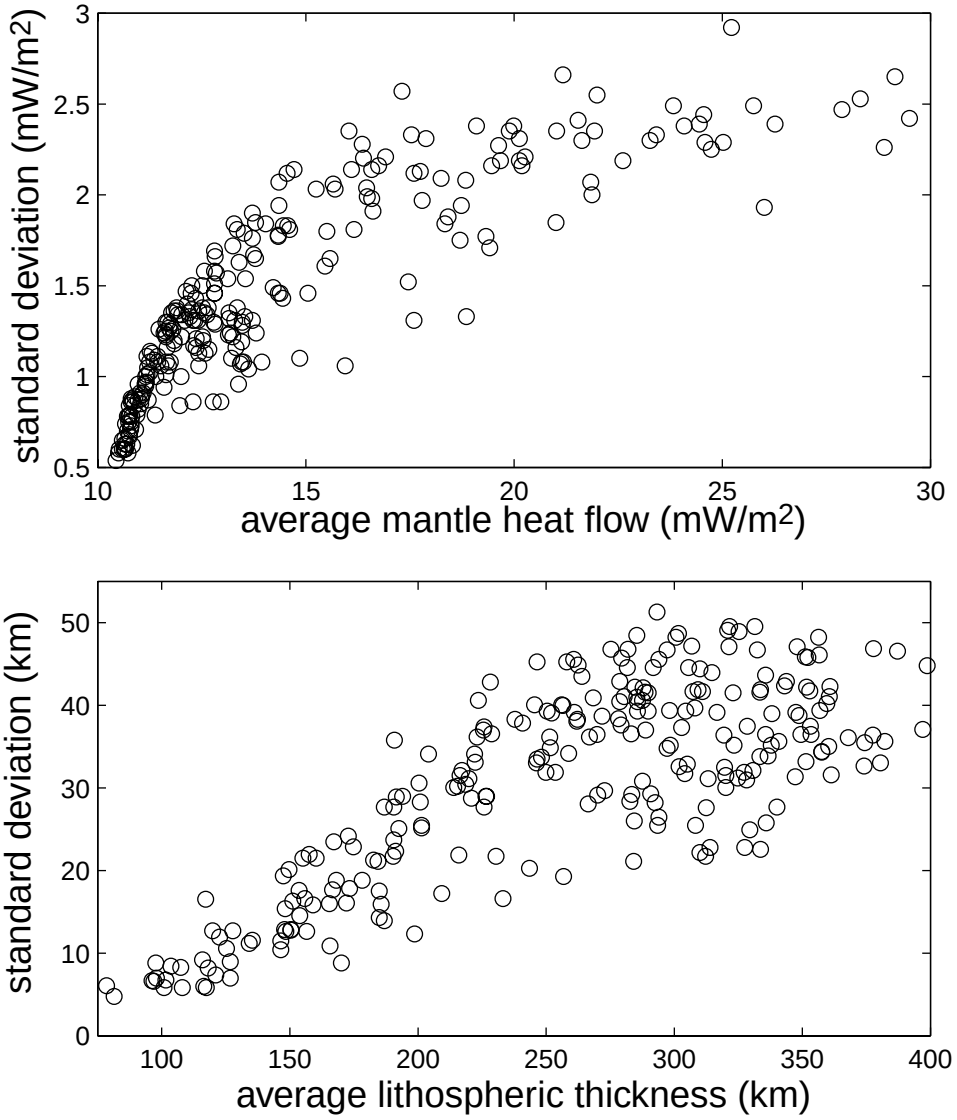

Figure 16. (Top) Estimated standard deviation of mantle heat flow plotted versus mantle heat flow. (Bottom) Estimated standard deviation of lithospheric thickness plotted versus lithospheric thickness. Values are taken at the model nodes on a $2^\circ \times 2^\circ$ grid across the region of study.

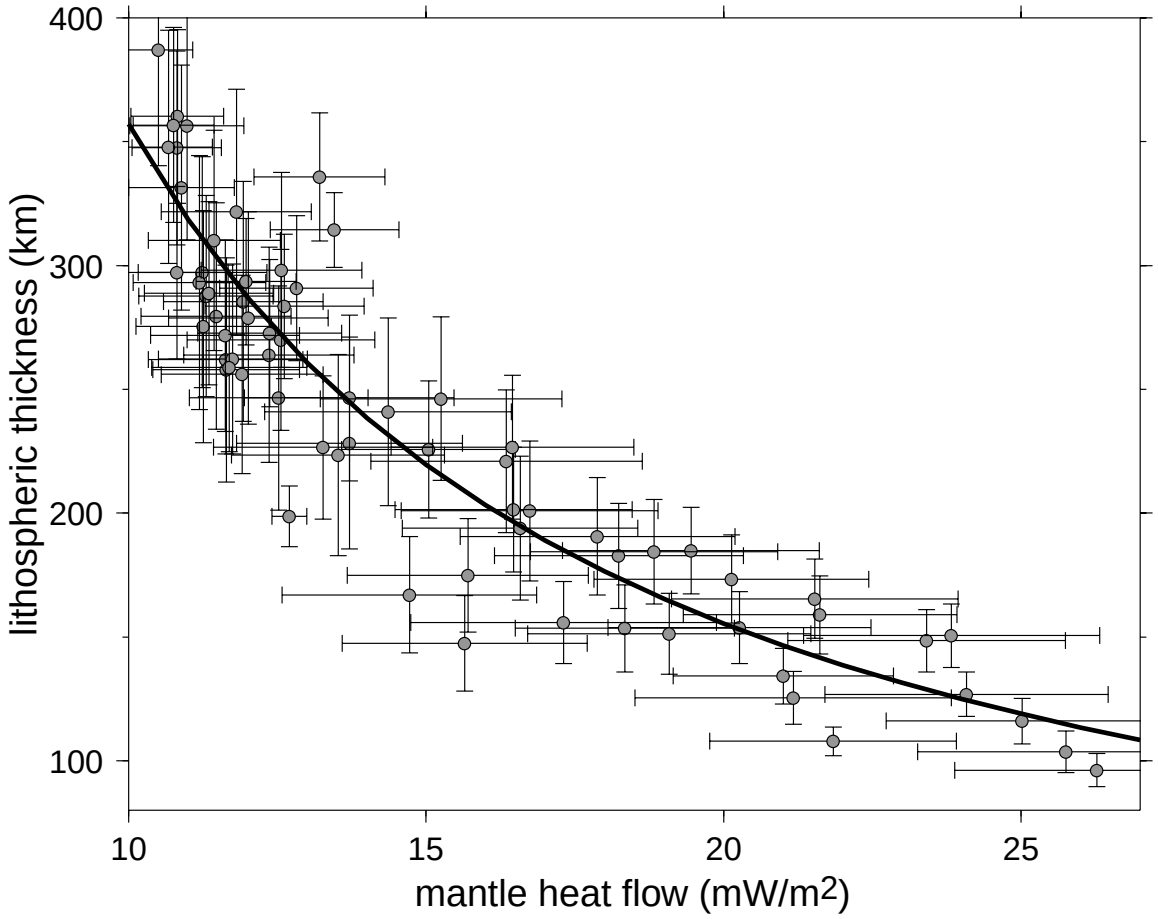

Figure 17. Lithospheric thickness (L) versus mantle heat flux (Q_M) taken from model nodes near the heat flow measurements shown in Figure 1. One standard deviation error bars in both L and Q_M are shown. The solid line is a power law curve that fits the data well ($L = 5660\ Q_M^{-1.2}$).